ACCOUNTS
of chemical research

New Generation "Nanohybrid Supercapacitor"

KATSUHIKO NAOI,*,†,‡ WAKO NAOI,‡ SHINTARO AOYAGI,†
JUN-ICHI MIYAMOTO,† AND TAKEO KAMINO†,§

†*Institute of Symbiotic Science & Technology, Tokyo University of Agriculture & Technology, 2-24-16 Naka-cho, Koganei, Tokyo 184-8558, Japan,* ‡*Divison of Art and Innovative Technology, K & W Inc, 1-3-16-901 Higashi, Kunitachi, Tokyo 186-0002, Japan, and* §*Advanced Microscope Systems Design Department, Hitachi High-Technologies Corp., 882 Ichige, Hitachinaka, Ibaraki 312-8504, Japan*

RECEIVED ON NOVEMBER 28, 2011

CONSPECTUS

To meet growing demands for electric automotive and regenerative energy storage applications, researchers all over the world have sought to increase the energy density of electrochemical capacitors. Hybridizing battery–capacitor electrodes can overcome the energy density limitation of the conventional electrochemical capacitors because they employ both the system of a battery-like (redox) and a capacitor-like (double-layer) electrode, producing a larger working voltage and capacitance. However, to balance such asymmetric systems, the rates for the redox portion must be substantially increased to the levels of double-layer process, which presents a significant challenge. An *in situ* material processing technology called "ultracentrifuging (UC) treatment" has been used to prepare a novel ultrafast $Li_4Ti_5O_{12}$ (LTO) nanocrystal electrode for capacitive energy storage.

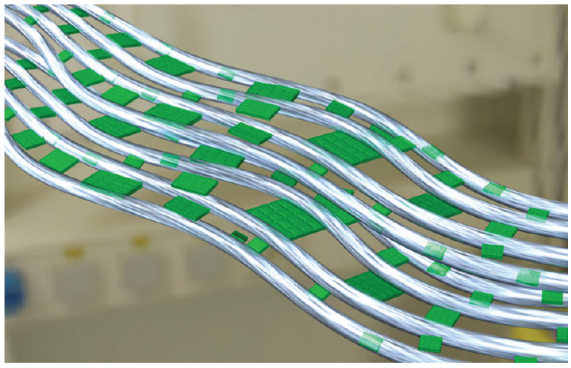

This Account describes an extremely high-performance supercapacitor that utilizes highly optimized "nano-nano-LTO/carbon composites" prepared via the UC treatment. The UC-treated LTO nanocrystals are grown as either nanosheets or nanoparticles, and both have hyperlinks to two types of nanocarbons: carbon nanofibers and supergrowth (single-walled) carbon nanotubes. The spinel structured LTO has been prepared with two types of hyperdispersed carbons. The UC treatment at 75 000G stoichiometrically accelerates the *in situ* sol–gel reaction (hydrolysis followed by polycondensation) and further forms, anchors, and grafts the nanoscale LTO precursors onto the carbon matrices. The mechanochemical sol–gel reaction is followed by a short heat-treatment process *in vacuo*. This immediate treatment with heat is very important for achieving optimal crystallization, inhibiting oxidative decomposition of carbon matrices, and suppressing agglomeration. Such nanocrystal composites can store and deliver energy at the highest rate attained to this date. The charge–discharge profiles indicate a very high sustained capacity of 80 mAh g^{-1} at an extremely high rate of 1200 C.

Using this ultrafast material, we assembled a hybrid device called a "nanohybrid capacitor" that consists of a Faradaic Li-intercalating LTO electrode and a non-Faradaic AC electrode employing an anion (typically BF_4^-) adsorption–desorption process. The "nanohybrid capacitor" cell has demonstrated remarkable energy, power, and cycleability performance as an electrochemical capacitor electrode. It also exhibits the same ion adsorption–desorption process rates as those of standard activated carbon electrodes in electrochemical capacitors. The new-generation "nanohybrid capacitor" technology produced more than triple the energy density of a conventional electrochemical capacitor. Moreover, the synthetic simplicity of the high-performance nanostructures makes it possible to scale them up for large-volume material production and further applications in many other electrochemical energy storage devices.

1. Introduction

Energy storage devices are some of the most promising and important environmental technologies that are highly influential in advancing our civilization's abilities and standard of living.[1−3] Specifically, electrochemical capacitors are efficient energy storage devices that exhibit long

Published on the Web 03/20/2012 www.pubs.acs.org/accounts
10.1021/ar200308h

lifespans and rapid charging and discharging.[4−10] Thus, the capacitor technology is regarded as a promising means for storing electricity.[1−6] This technology has an additional advantage of increasing effectiveness when combined with renewable (wind and solar) energy sources.[6,11] In recent years, electrochemical capacitors have been vigorously researched in hopes to improve their energy density. However, since electrochemical capacitors generally have low energy densities (below 10 Wh L^{-1}), their uses are limited and cannot fully meet performance demands required by existing electrical equipment and electronic devices. In the case of automobiles and smart grids, new energy storage devices necessitate both the attributes of lithium ion batteries, allowing high energy density, and the characteristics of electrochemical capacitors of fast charge−discharge rates in order to optimize the energy and power densities.

Such hybrid approaches can overcome the energy density limitation of conventional electrochemical capacitors because they employ both the system of a battery-like (Faradaic) electrode and a capacitor-like (non-Faradaic) electrode, producing a larger working voltage and capacitance.[6,10] These systems can double or triple the energy density up to 20−30 Wh L^{-1} compared with that of conventional electrochemical capacitors. However, the ion exchange rates at the Faradaic electrodes must be increased to the levels of non-Faradaic electrodes in order to balance the two systems.

2. New Nanotech to New Capacitor Concept

To meet these demands, state-of-the-art nanomaterials, specifically carbon nanotubes, are actively applied to form composites enhancing the energy−power capability effectively.[12,13] The authors developed and applied an original *in situ* material processing technology called "UC treatment" (UC stands for ultracentrifuging) to prepare an ultrafast $Li_4Ti_5O_{12}$ (LTO) electrode material (hereafter abbreviated as UC-LTO).[17−18] The UC treatment relies on centrifuging, which induces simultaneous synthesis of nanoscale oxide particles via a sol−gel reaction and as a result hybridizes, entangles, and confines these structures into carbon matrices.[14−16] We first applied this method for the preparation of nanodot hydrous RuO_2[14] for aqueous supercapacitors, which produced a 10-fold increase in capacitance (1000 F g^{-1}) over conventional activated carbon capacitor electrodes (100−140 F g^{-1}). By combining the established material selections for batteries and capacitors, the UC treatment enhances the cohesion of the two initially divergent principles into a novel hybrid concept (Figure 1) that is capable of meeting and even exceeding the current energy and power demands.

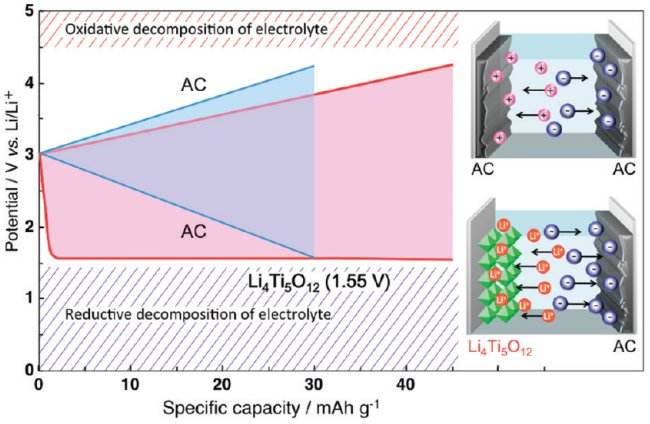

FIGURE 1. Configuration of nanohybrid capacitor. The device consists of a $Li_4Ti_5O_{12}$ (LTO) negative electrode combined with an activated carbon (AC) positive electrode. This is a hybrid system of a Faradaic Li-insertion LTO electrode and a non-Faradaic AC electrode employing an anion (typically BF_4^-) adsorption−desorption process. This configuration of the device will produce a larger working voltage and capacitance within the safe voltage range among oxidative and reductive decomposition of electrolytes. The nanohybrid capacitor (configured as LTO/AC) can produce a higher energy density compared with a conventional (AC/AC) electrochemical capacitor whose energy density is less than 10 Wh L^{-1}.

We focused on one of the Li^+ insertion compounds, LTO, which is a well-known Li-ion battery material. LTO has the following advantages: (1) high Coulombic efficiency close to a theoretical capacity of 175 mAh g^{-1},[19−21] (2) thermodynamically flat discharge profile at 1.55 V vs Li/Li^+,[20,22] (3) zero-strain insertion that provides little volume change during charge and discharge,[19,20] and (4) safety with little electrolyte decomposition (no SEI (solid electrolyte interface) formation and no gas evolution).[23] Amatucci et al. first introduced the LTO/AC system as a possible battery−capacitor hybrid energy device.[24] However, conventional LTO electrodes have significant drawbacks such as low power characteristics that stem from an inherently low Li^+ diffusion coefficient (<10^{-6} cm^2 s^{-1}) and poor electronic conductivity (<10^{-13} Ω^{-1} cm^{-1}).[23,24]

3. Nanofabrication and Nanohybidization

In situ synthesis of the nano-LTO precursor and simultaneous hybridization of two kinds of carbon matrices, carbon nanofiber (CNF) and supergrowth carbon nanotube (SGCNT), was carried out using UC treatment (Figure 2).[14,15] Tetrabutyl titanate [$Ti(OC_4H_9)_4$], as a titanium source, was dissolved in isopropyl alcohol. Then, lithium acetate, as a lithium source, was dissolved into a solution of isopropyl alcohol, deionized water, and acetic acid. A mechanochemical agitation was applied to the carbon-containing mixture for 5 min at

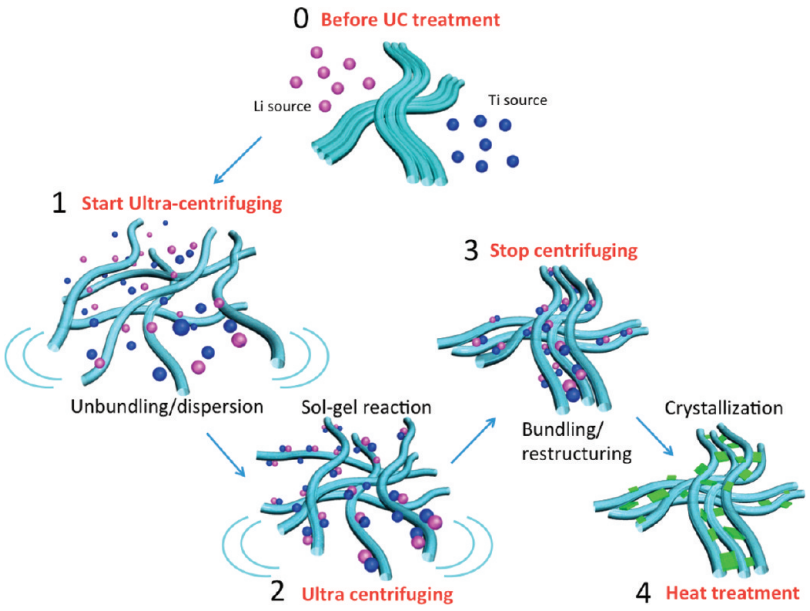

FIGURE 2. Concept of ultracentrifuging (UC) treatment. The UC treatment involves a simple one-pod rapid generation scheme yielding a series of optimized "nano-nano composites", capable of storing and delivering energy at the highest sustained capacity with remarkable C rates. With this method, we can enhance the rate of many Li-insertion compounds for batteries and utilize them as alternative capacitor electrodes. The UC treatment is a build-up synthetic scheme involving the following 4 steps: (0) starting materials, namely, carbon matrix (CNF or SGCNT) and Ti and Li sources, are premixed; (1) starting ultracentrifugation, which initiates unbundling of the carbon matrix for maximum dispersion in order to obtain the highest probability of contact with reactant species; (2) sol−gel reaction takes place and produces LTO precursor *in situ* on carbon; (3) termination of ultracentrifuging induces rebundling and restructuring of the carbon matrix to form a "nano-nano composite", highly dispersed with nanoscale LTO precursors; this process simultaneously produces a mesopore network (that acts as an electrolyte reservoir) of interstices created between the carbon matrixes due to the trapped LTO precursors; (4) post-centifugation heat treatment effectively completes the crystallization process, producing LTO spinel structures without crystal growth (further description in Figure 5).

75 000G under the same conditions described elsewhere.[14,16] The precursor composites were obtained after drying the resultant gel at 80 °C for 17 h *in vacuo*, then calcinating for a short duration of 3 min at 900 °C *in vacuo*. The weight ratio of LTO/carbon was controlled by the dosed molar ratios of the Li source and the Ti source. A CNF, CO-derived carbon nanotube obtained from JEMCO, is a tubular carbon fiber consisting of 10−20 graphene layers that are synthesized through the decomposition of carbon-containing gases via chemical vapor deposition.[31] The diameter and specific surface area (SSA) of the received CNFs are 15−20 nm and 400 $m^2 g^{-1}$, respectively. A SGCNT, obtained from National Institute of Advanced Industrial Science and Technology (AIST), was used without further purification.[27−30] The SSA measured for the resulting LTO/CNF and LTO/SGCNT composites show typically 99 and 177 $m^2 g^{-1}$, respectively.

We used our newly synthesized UC-LTO/carbon composites as the negative electrode in combination with activated carbon as the positive electrode in configuring the nanohybrid capacitor. As described later, this new capacitor device results in an extremely high energy performance at the same level of power capability (cycled >10 000 cycles) that exceeds those of conventional electrochemical capacitors.

3.1. Nanosheet LTO/CNF Composites. The spinel-structured LTO has thus been prepared with two types of hyperdispersed carbons, CNF and SGCNT. As described in our previous papers,[14−16] the UC treatment at 75 000G stoichiometrically accelerates the *in situ* sol−gel reaction (hydrolysis followed by polycondensation) and further forms, anchors, and grafts the nanoscale LTO precursors onto the carbon matrices. The mechanochemical sol−gel reaction is followed by a short heat-treatment process *in vacuo*. The instantaneity of the heat treatment is of utmost importance in achieving high crystallization, inhibiting oxidative decomposition of carbon matrices, and suppressing agglomeration. In our current research, we further optimized this annealing process in order to avoid any oxidative decomposition of carbon. In order to characterize the stoichiometry of the composites, thermal analysis was performed in a temperature range of 25−1000 °C under air atmosphere (100 mL min^{-1}) using a SII EXSTAR 6000 TG/DTA 6300 thermal analyzer with a heating rate of 5 °C min^{-1}. The weight ratio of LTO to carbon matrices

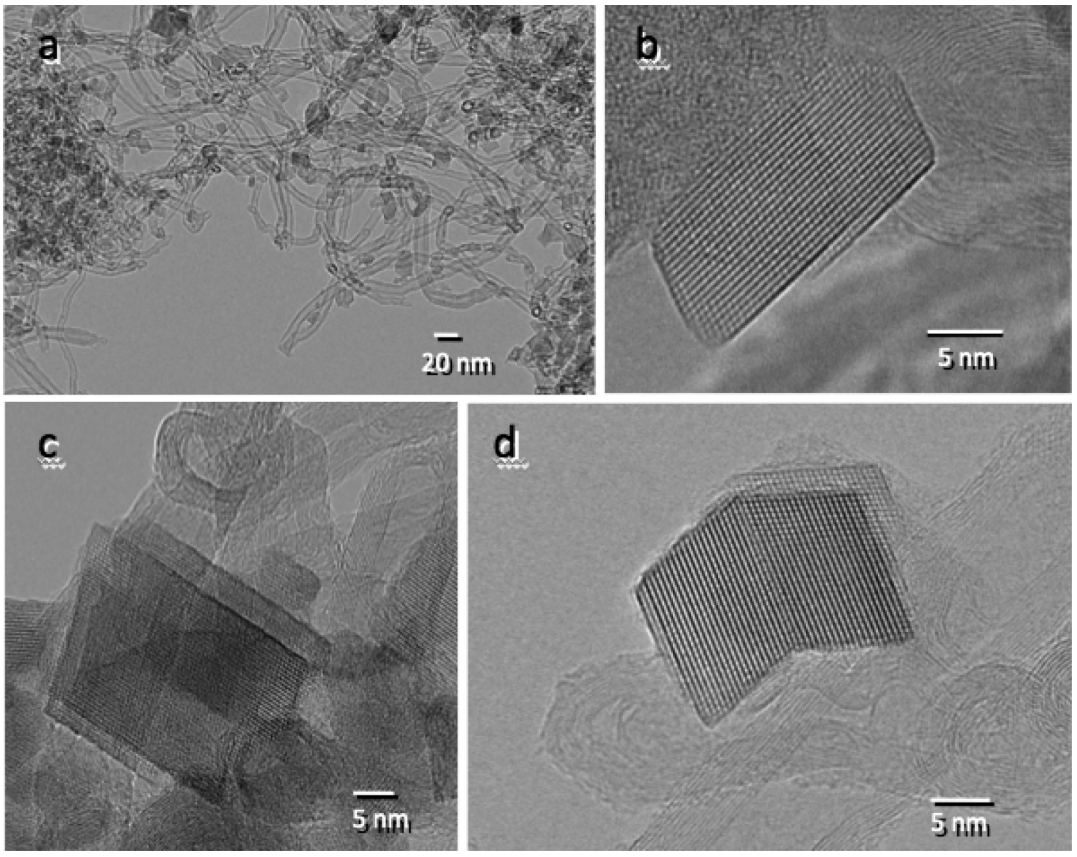

FIGURE 3. HRTEM images of UC-LTO/CNF nanosheets. (a) Overall view of the UC-LTO/CNF (weight ratio of LTO to CNF = 70:30). (b) HRTEM image of UC-LTO/CNF nanosheet. (c) HRTEM image of UC-LTO nanosheet, clearly demonstrating the 2D-LTO crystals. (d) HRTEM image of two interconnected LTO twin crystals called a "nanobook".

was based on the weight of dosed titanium alkoxide before the UC treatment. Annealing at 700 °C under N_2 for 3 min was enough to crystallize the LTO/CNF precursors. In order to characterize the composites, X-ray diffraction, Raman spectroscopy (Jasco NSR-2100, excited by 514 nm Ar laser), and HRTEM were used in this study. X-ray powder diffraction (Rigaku SmartLab, Cu Kα radiation $\lambda = 1.54056$ Å, operating at 45 kV−200 mA) was used to characterize the crystalline structure and crystallite diameter of the LTO in the composites.

The XRD peaks for some possible impurities such as TiO_2, Li_2CO_3, and Li_2TiO_3[25,26] were below the detection limits, and the major phase was the spinel-LTO and carbon matrix.

HRTEM (Hitachi H-9500, 300 kV) was used for characterization of the UC-LTO/carbon composites. A sample was ultrasonically dispersed in ethanol for 5 min and dropped onto a microgrid (Okenshoji, Type B Cu150 μm). Figure 3a is a HRTEM image of the obtained LTO/CNF, which displays the high dispersion of LTOs among the CNF network. Figure 3b,c shows magnified high-resolution images that confirm planar LTO crystals grown two-dimensionally on the CNF. These images demonstrate that the 2D LTO nanosheet is nucleated and developed on the CNF and is firmly attached before the annealing process. As a result of the fast Fourier transform (FFT) analysis on TEM images, the lattice of the LTO crystals was composed with *d* spacing of 4.81 Å, indicative of the spinel (111) plane. When the annealing process is shortened, the (111) plane is able to develop both at a rapid pace and in shape with its surrounding carbon matrix. This can be clearly observed in Figure 3c. The growth direction of the 2D LTO crystals follows the contour of the CNF matrix to the extent that a very peculiar structure of two interconnected LTO nanosheets in the shape of an open book was formed (Figure 3d). This "nanobook" of folded LTO/CNF layers suggests that the (111) plane of the LTO nanosheet rapidly changed its direction of growth by about 120° in shape with the contour of the its attached CNF matrix.

3.2. Hyperdispersed LTO/SGCNT Composites. We replaced the CNF with SGCNT, a single-walled carbon nanotube synthesized through a supergrowth method[27−30] (Figure 4a) as the matrix for the LTO composite. We expected

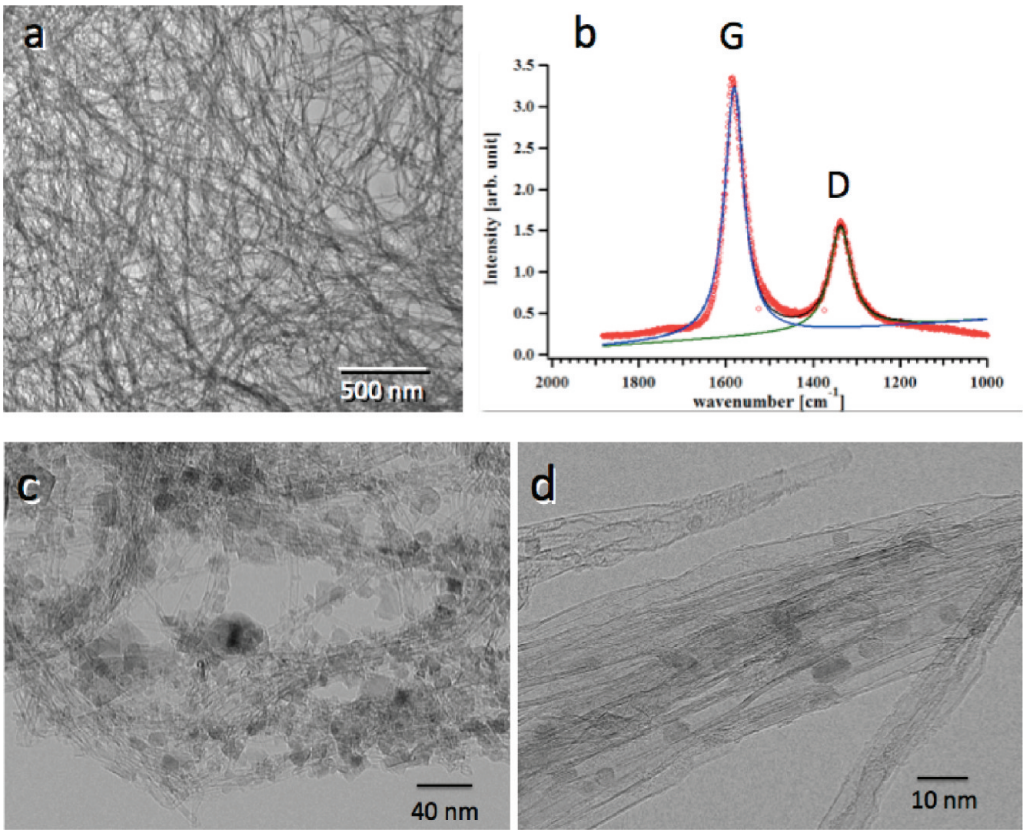

FIGURE 4. TEM observations of SGCNT and UC-LTO/SGCNT. (a) TEM image of a well-dispersed and unbundled pristine SGCNT (3−5 nm in diameter, specific surface area 600 $m^2 g^{-1}$). (b) Raman spectroscopy of the same SGCNT, showing a fairly high disorder ratio ($I_G/I_D = 2.4$). This is an indication that the SGCNT used here has abundant anchoring sites for LTO to nucleate. (c) HRTEM image of UC-LTO/SGCNT (the weight ratio of LTO to SGCNT = 80:20), exhibiting highly dispersed LTO particles of about 2−20 nm in diameter within the SGCNT network. (d) HRTEM of UC-LTO/SGCNT (85:15) composite. The high-magnification images confirmed the existence of LTO particles not only within the interstitial spaces of the SGCNT bundles but also inside the single-walled carbon nanotubes in their highly crystalline states. By use of SGCNT in our UC treatment, the ratio of LTO to SGCNT can be maximized to 90% while still maintaining the LTO crystals in small-nucleated and single-nanosized dimension.

the SGCNT to be a better supporting material due to its high specific surface area, high elemental purity, and high electrical conductivity.[30] The typical I_G/I_D ratio of the SGCNT used specifically for the UC nanohybridization was 2.4, as obtained through Raman spectroscopy (Figure 4b). This indicates that compared with the normal SGCNT (I_G/I_D is typically 12−14) as reported previously,[27] it has a fairly high content of defects acting as optimal anchoring sites for the LTO precursors to nucleate. Figure 4c,d shows HRTEM images of a high loading LTO/SGCNT (80% LTO) in which highly dispersed LTO particles of about 2−20 nm in diameter can be clearly observed in the SGCNT network. In addition, the high-magnification images confirmed the existence of the LTO particles not only within the interstitial spaces of the SGCNT bundles but also inside the tubes in their highly crystalline states (Figure 4d). By use of SGCNT in our UC treatment, the ratio of LTO to SGCNT was increased to 90% while still maintaining the LTO nanocrystals in single digit size. This allows for further enhancement in both energy and power capabilities.

4. Crystallization Process of Nanoprecursor UC-LTO Particle

Real-time monitoring of the LTO annealing process was conducted through the use of *in situ* HRTEM (Figure 5). For a real-time monitoring, the sample was mounted on a special tungsten (W-wire) specimen heating holder,[32] allowing us to precisely control its temperature through the adjustment of the DC current. The temperature was within ±20 °C precision that was independently calibrated using a pyrometer.[33] The dried LTO/SGCNT (weight ratio = 80:20) precursors were subjected to preheating at 400 °C for 30 min and then elevated to 670 °C *in vacuo* in the TEM chamber. A sequence of high-resolution electron micrographs shows the *in situ* crystallization of UC-LTO/SGCNT at 670 °C. What becomes immediately apparent is the fact that despite

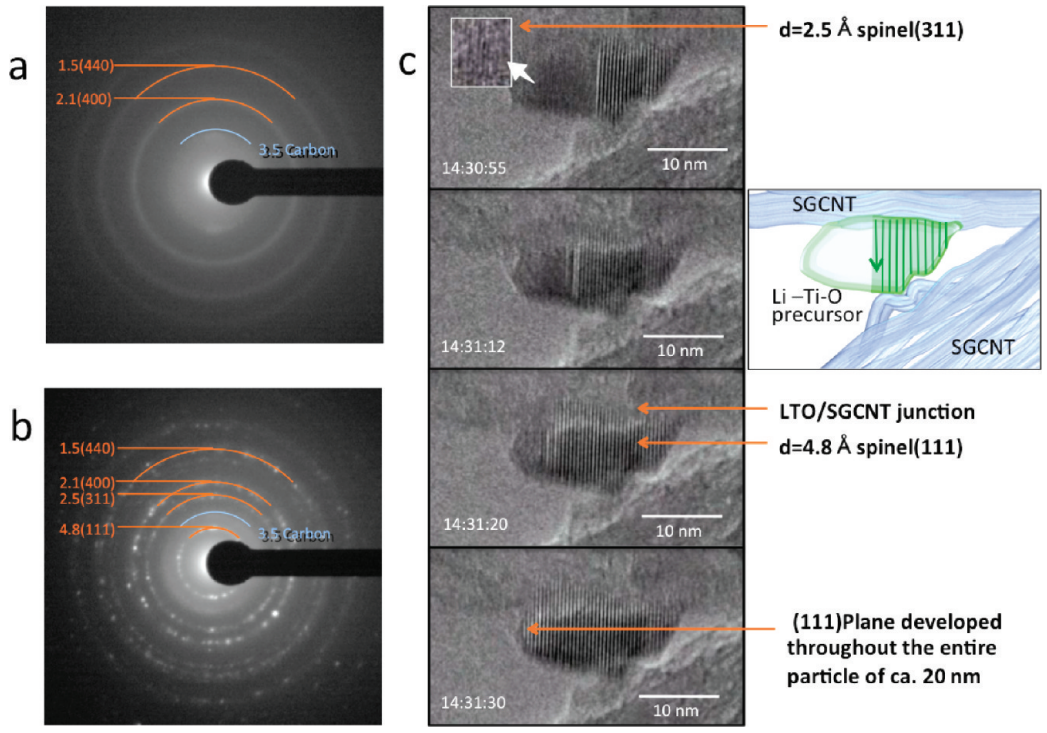

FIGURE 5. *In situ* real-time TEM observation during crystallization process of a UC-LTO/SGCNT. (a) Electron diffraction patterns of a preheated precursor at 400 °C, showing its precrystallized state. (b) Electron diffraction patterns of the same sample after annealing at 670 °C. The rings and spots correspond to the *d*-spacing in Å (lattice plane) for the spinel structures of LTO and carbon. The *d* spacings of 4.8, 2.5, 2.1, and 1.5 Å correspond to the lattice planes of (111), (311), (400), and (440), respectively. (c) Magnified views of selected HRTEM images during a consecutive real-time monitoring of the focused UC-treated LTO/SGCNT particle through its process of full crystallization. The development of the vertical (111) fringes can be seen from right to left throughout one particle. Within 45 s, a single UC-LTO/SGCNT precursor particle was fully crystallized into a spinel LTO.

crystallization, no growth in size of the LTO was observed. This can be partially explained due to its confinement within the cavity-crated entanglement of the carbon nest as well as other optimal accommodations during the annealing process.

Electron diffraction (ED) analysis was performed during preannealing at 400 °C (Figure 5a) and postannealing at 670 °C (Figure 5b) to confirm the formation of the LTO crystal structures and the unchanged presence of the SGCNT. The postannealing ED pattern seen in Figure 5b clearly indicates the presence of face-centered cubic spinel structures with a $Fd\bar{3}m$ space group.[19,20]

To further examine the crystallization process, we recorded in real-time the partial crystallization of a LTO particle. Figure 5c shows magnified views of selected HRTEM images during the monitoring period, focusing on one LTO precursor particle for 45 s through its process into a fully crystallized spinel structure. Recorded after the formation of roughly half the crystal, the crystallization process proceeded very rapidly with the immediate formation of a fully crystallized particle of 20 nm in diameter within a mere 45 s. Approximately every 4.8 Å, we observed a new fringe, suggesting the formation of a spinel (111) plane, characterized by its *d* spacing of 4.8 Å. In its process of development, we also observed traces of (311) planes with smaller *d* spacing of 2.5 Å immediately prior to the formation of the (111) planes.

5. Performance of Nanohybrid Supercapacitor

Electrochemical characteristics were evaluated using a half-cell electrode setup (Li/(UC-LTO/carbon)). The half-cell was assembled with a Li metal electrode and a LTO/carbon electrode, using a 2032 coin-type cell. The electrolyte was a mixture of ethylene carbonate (EC) and dimethyl carbonate (DMC) containing 1.0 M lithium tetrafluoroborate ($LiBF_4$) as an electrolyte salt. The LTO/carbon electrode was prepared by mixing 80% of the composite and 20% of poly(vinylidene fluoride) (PVDF) in *N*-methylpyrrolidone. The mixture was coated on a Cu foil (current collector) and dried at 150 °C *in vacuo*. The thickness of the LTO/carbon electrode was ca. 20 μm, corresponding to a loading weight of ca. 1 mg. Charge–discharge tests were performed under CC-mode between 1.0 and 3.0 V vs Li/Li^+ at several current density ranges.

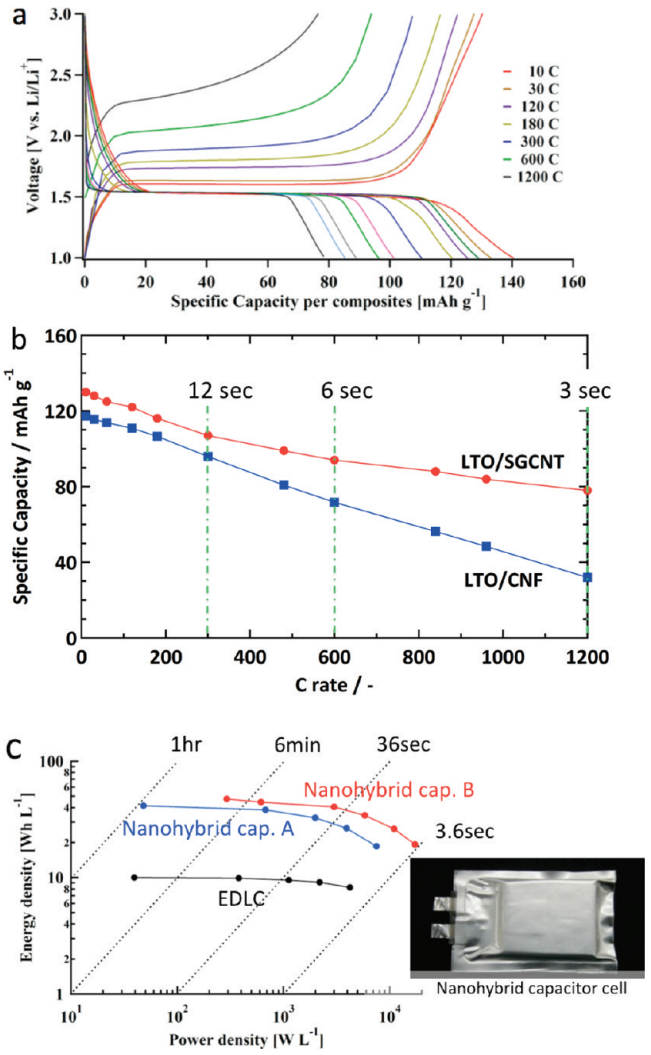

FIGURE 6. Supercapacitor performance of nanohybrid capacitor using UC-LTO/CNF and UC-LTO/SGCNT. (a) Charge–discharge profiles for a LTO/SGCNT electrode, exhibiting unusually high charge retention at C rates in the higher ranges of 300–1200 C. Such a remarkably high response of the LTO composite is due to the nanosizing of the LTO particles and the mesopore network of the carbon nanofibers that allows an entanglement effect of the nano-LTO and nano-SGCNT. This enables hyperdiffusivity and accessibility of the electrolyte, leading to an increase in electrical conductivity. (b) Delivered specific capacity as a function of C rate for half-cell capacitors utilizing UC-LTO/CNF and UC-LTO/SGCNT. This demonstrates that the retention of specific capacity of UC-LTO/SGCNT at high C rates is even higher than that of UC-LTO/CNF. (c) Ragone plots for two full cell capacitors, nanohybrid capacitor A [UC-LTO/CNF (70:30)]/AC] and nanohybrid capacitor B [UC-LTO/SGCNT (80:20)/SGCNT]. A full cell for a normal EDLC (AC/1 M TEMABF$_4$/PC/AC) was employed as a reference and measured in the same conditions above.

Figure 6a shows the charge–discharge curves of the half-cell Li/UC-LTO/SGCNT between 10 and 1200 C. The dominant plateau was observed at 1.55 V (vs Li/Li$^+$), indicating the Li$^+$ intercalation–deintercalation of a spinel LTO.[19,21] A highly loaded LTO composite (with the LTO/SGCNT ratio of 80:20) showed a specific capacity of 130 mAh g^{-1} (per composite) at 10 C (1 C = 175 mAh g^{-1}). This value is ca. 93% of the theoretical capacity of LTO. Remarkably, the composite showed 107 mAh g^{-1} at 300 C and 78 mAh g^{-1} (60% retention) even at 1200 C. In other words, high retention of the LTO specific capacity is attained despite such high C rates in the higher ranges above 300 C.

Figure 6b further demonstrates that the retention of specific capacity of UC-LTO/SGCNT at high C rates is even higher than that of UC-LTO/CNF. Such a remarkably high rate capability of the LTO composite is due to the unusually small nanocrystalline LTO particles that increase electrochemical utilization and the mesopore network of the CNF that allows an entanglement effect of the nano-LTO and nano-SGCNT. These two aspects enable hyperdiffusivity and accessibility of the electrolyte, thus enhancing ionic conductivity. Such LTO composites (both UC-LTO/CNF and UC-LTO/SGCNT) were utilized in combination with two kinds of positive electrodes, activated carbon and SGCNT, in creating full laminate cells of nanohybrid capacitors. The nanohybrid capacitors A and B comprise [UC-LTO/CNF (70:30)]/1 M LiBF$_4$/EC+DMC/AC and [UC-LTO/SGCNT (80:20)]/1 M LiBF$_4$/EC+DMC/SGCNT, respectively, and were tested for their energy–power performances in the same conditions as a reference EDLC (AC/1 M LiBF$_4$/PC/AC) cell. Figure 6c shows Ragone plots for the nanohybrid capacitor cells A and B and EDLC cell obtained from the charge–discharge curves (10–300 C). In a low power density range of 0.1–1 kW L^{-1}, the nanohybrid capacitors show energy densities as high as 28–30 Wh L^{-1}, which is a value comparable to that of Li-ion capacitors.[6,10] Even at a high power density of 6 kW L^{-1}, the energy densities of the nanohybrid capacitors remain at 15 Wh L^{-1}, which is double that of conventional electrochemical capacitors. The result reveals that nanohybrid capacitor A can provide 3 times higher energy than the existing alternatives in both ranges of low power density (0.1–1 kW L^{-1}) and nanohybrid capacitor B showed 4.5 times higher energy density than the conventional EDLC cell even at high power density of 1–6 kW L^{-1}. It should be noted however that the utilization and a real application of the SGCNT in a large-scale practical supercapacitor device should await its further cost reduction by nearly a factor of 1/10. However, the nanohybrid capacitor configuration as a new generation supercapacitor system can be one of the realizable alternatives because the SGCNT is only used in some portion, for example, 20%, within the whole composite electrode materials (LTO/SGCNT = 80:20 as shown in Figure 6). This suggests a strong strategy to save the cost of capacitor

devices by reducing the dosage of the expensive SGCNT material.

6. Concluding Remarks

The UC-treated LTO/carbon composites described in this Account are newly synthesized materials that we utilized in configuring the nanohybrid capacitor, which effectively increases the energy density of electrochemical storage devices. The "nanohybrid capacitor" achieves a high energy density comparable to Li-ion capacitors but with an increased stability and safety while operating at very high current densities. This new hybrid technology is able to meet the energy and power demands for a variety of applications ranging from microelectronic devices to electrical vehicles and exhibits a breakthrough improvement for future energy storage devices.

The authors are indebted to K. Hata, AIST Japan, and S. Iijima (Meijo University, Japan) for supplying SGCNT through NEDO project, Carbon Nanotube Capacitor Project (2006–2011). K.N. is grateful to Y. Gogotsi and B. Dyatkin (Drexel University, U.S.A.) and P. Simon (Paul Sabatier University, France) for valuable discussions. Special thanks to S. Ishimoto (Nippon Chemi-con Corp.) for fabricating test capacitor cells for obtaining supercapacitor performances (Ragone plots).

BIOGRAPHICAL INFORMATION

Katsuhiko Naoi is a professor of chemistry at the Institute of Symbiotic Science & Technology at Tokyo University of Agriculture & Technology (TAT). With a Ph.D. from Waseda University, Tokyo, his research interests are advanced supercapacitors, future nanobatteries, and energy, environmental, and materials science.

Wako Naoi founded in 2002 K & W Inc., a TAT venture company dealing with "Energy Solutions for the Future". She serves as a CEO of the company also manipulating TEM and SEM for nanostructure characterization. She received her B.A. at Doshisha University in Kyoto and her major was Art and Art History.

Shintaro Aoyagi received his M.S. at TAT in 2010. He joined HONDA Motors Company working on HEV battery technology.

Jun-ichi Miyamoto received his Ph.D. in 2005 from Chiba University. He worked for BEL Japan Inc. for 7 years. From 2002, he studied porous carbonaceous materials by adsorption technique in Chiba University from theoretical and experimental aspects. He joined TAT in 2010 and started investigating supercapacitors.

Takeo Kamino is a distinguished visiting professor at Tokyo University of Agriculture and Technology (TAT). He also acts as a technical advisor of Hitachi High-Technologies Corp., a scientific instruments manufacturer. With a Ph.D. from Ibaraki University, his interests are development and application of environmental transmission electron microscopy techniques.

FOOTNOTES

*E-mail: k-naoi@cc.tuat.ac.jp.
The authors declare no competing financial interest.

REFERENCES

1 Simon, P.; Gogotsi, Y. Materials for electrochemical capacitors. *Nat. Mater.* **2008**, *7*, 845.
2 Chmiola, J.; Largeot, C.; Taberna, P.-L.; Simon, P.; Gogotsi, Y. Monolithic carbide-derived carbon films for micro-supercapacitors. *Science* **2010**, *328*, 480–483.
3 Gao, W.; Singh, N.; Song, L.; Liu, Z.; Reddy, A. L. M.; Ci, L.; Vajtai, R.; Zhang, Q.; Wei, B.; Ajayan, P. M. Direct laser writing of micro-supercapacitors on hydrated graphite oxide films. *Nat. Nanotechnol.* **2011**, *6*, 496–500.
4 Pech, D.; Brunet, M.; Durou, H.; Huang, P.; Mochalin, V.; Gogotsi, Y.; Taberna, P.-L.; Simon, P. Ultrahigh-power micrometre-sized supercapacitors based on onion-like carbon. *Nat. Nanotechnol.* **2010**, *5*, 651–654.
5 Lee, S. W.; Yabuuchi, N.; Gallant, B. M.; Chen, S.; Kim, B.-S.; Hammond, P. T.; Shao-Horn, Y. High-power lithium batteries from functionalized carbon-nanotube electrodes. *Nat. Nanotechnol.* **2010**, *5*, 531–537.
6 Burke, A. Ultracapacitors: Why, how, and where is the technology. *J. Power Sources* **2000**, *91*, 37–50.
7 Pandolfo, A. G.; Hollenkamp, A. F. Carbon properties and their role in supercapacitors. *J. Power Sources* **2006**, *157*, 11–27.
8 Kötz, R.; Carlen, M. Principles and applications of electrochemical capacitors. *Electrochim. Acta* **2000**, *45*, 2483–2498.
9 Plitz, I.; Dupasquier, A.; Badway, F.; Gural, J.; Pereira, N.; Gmitter, A.; Amatucci, G. G. The design of alternative nonaqueous high power chemistries. *Appl. Phys. A: Mater. Sci. Process.* **2006**, *82*, 615–626.
10 Naoi, K.; Simon, P. New materials and new configurations for advanced electrochemical capacitors. *Interface* **2008**, *17*, 34–37.
11 Lang, X.; Hirata, A.; Fujita, T.; Chen, M. Nanoporous metal-oxide hybrid electrodes for electrochemical supercapacitors. *Nat. Nanotechnol.* **2011**, *6*, 232–236.
12 Wang, Q.; Wen, Z.; Li, J. Carbon nanotube/TiO_2 nanotube hybrid supercapacitors. *J. Nanosci. Nanotechnol.* **2007**, *7*, 3328–3331.
13 Zhang, W.-D.; Xu, B.; Jiang, L. C. Functional hybrid materials based on carbon nanotubes and metal oxides. *J. Mater. Chem.* **2010**, *20*, 6383–6391.
14 Naoi, K.; Ishimoto, S.; Ogihara, N.; Nakagawa, Y.; Hatta, S. Encapsulation of nanodot ruthenium oxide into KB for electrochemical capacitors. *J. Electrochem. Soc.* **2009**, *156*, A52–59.
15 Naoi, K.; Ishimoto, S.; Isobe, Y.; Aoyagi, S. High-rate nano-crystalline $Li_4Ti_5O_{12}$ attached on carbon nano-fibers for hybrid supercapacitors. *J. Power Sources* **2010**, *195*, 6250–6254.
16 Naoi, K. Nanohybrid capacitor: The next generation electrochemical capacitors. *Fuel Cells* **2010**, *10*, 825–833.
17 Huang, S.; Wen, Z.; Zhu, X.; Gu, Z. Preparation and electrochemical performance of Ag doped $Li_4Ti_5O_{12}$. *Electrochem. Commun.* **2004**, *6*, 1093–1097.
18 Kim, J.; Cho, J. Spinel $Li_4Ti_5O_{12}$ nanowires for high-rate Li-ion intercalation electrode. *Electrochem. Solid-State Lett.* **2007**, *10*, A81–84.
19 Ohzuku, T.; Ueda, A.; Yamamoto, N. Zero-strain insertion material of $Li[Li_{1/3}Ti_{5/3}]O_4$ for rechargeable lithium cells. *J. Electrochem. Soc.* **1995**, *142*, 1431–1435.
20 Thackeray, M. M. Structural considerations of layered and spinel lithiated oxides for lithium ion batteries. *J. Electrochem. Soc.* **1995**, *142*, 2558–2563.
21 Jansen, A. N.; Kahaian, A. J.; Kepler, K. D.; Nelson, P. A.; Amine, K.; Dees, D. W.; Vissers, D. R. Development of a high-power lithium-ion battery. *J. Power Sources* **1999**, *81–82*, 902–905.
22 Scharner, S.; Weppner, W.; Schmind-Beurmann, P. Evidence of Two-Phase Formation upon Lithium Insertion into $Li_{1.33}Ti_{1.67}O_4$ spinel. *J. Electrochem. Soc.* **1999**, *146*, 857–861.
23 Shu, J. Study of the interface between $Li_4Ti_5O_{12}$ electrodes and standard electrolyte solutions in 0.0–5.0 V. *Electrochem. Solid-State Lett.* **2008**, *11*, A238–240.
24 Amatucci, G. G.; Badway, F.; Pasquier, A. D.; Zheng, T. An asymmetric hybrid nonaqueous energy storage cell. *J. Electrochem. Soc.* **2001**, *148*, A930–939.
25 Takai, S.; Kamata, M.; Fujiine, S.; Yoneda, K.; Kanda, K.; Esaka, T. Diffusion coefficient measurement of lithium ion in sintered $Li_{1.33}Ti_{1.67}O_4$ by means of neutron radiography. *Solid State Ionics* **1999**, *123*, 165–172.
26 Chen, C. H.; Vaughey, J. T.; Jansen, A. N.; Dees, D. W.; Kahaian, A. J.; Goacher, T.; Thackeray, M. M. Studies of Mg-substituted $Li_{4-x}MgxTi_5O_{12}$ spinel electrodes ($0 \leq x \leq 1$) for lithium batteries. *J. Electrochem. Soc.* **2001**, *148*, A102–104.

27 Hata, K.; Futaba, D. N.; Mizuno, K.; Namai, T.; Yumura, M.; Iijima, S. Water-assisted highly efficient synthesis of impurity-free single-walled carbon nanotubes. *Science* **2004**, *306*, 1362–1364.

28 Yuge, R.; Miyawaki, J.; Ichihashi, T.; Kuroshima, S.; Yoshitake, T.; Ohkawa, T.; Aoki, Y.; Iijima, S.; Yudasaka, M. Highly efficient field emission from carbon nanotube–nanohorn hybrids prepared by chemical vapor deposition. *ACS Nano* **2010**, *4*, 7337–7343.

29 Hiraoka, T.; Izadi-Najafabadi, A.; Yamada, T.; Futaba, D. N.; Yasuda, S.; Tanaike, O.; Hatori, H.; Yumura, M.; Iijima, S.; Hata, K. Compact and light supercapacitor electrodes from a surface-only solid by opened carbon nanotubes with 2200 m^2 g^{-1} surface area. *Adv. Funct. Mater.* **2010**, *20*, 422–428.

30 Izadi-Najafabadi, A.; Futaba, D. N.; Iijima, S.; Hata, K. ion diffusion and electrochemical capacitance in aligned and packed single-walled carbon nanotubes. *J. Am. Chem. Soc.* **2010**, *132*, 18017–18019.

31 Zou, J. H.; Sui, Z. J.; Li, P.; Chen, D.; Dai, Y. C.; Yuan, W. K. Structural characterization of carbon nanofibers formed from different carbon-containing gasses. *Carbon* **2006**, *44*, 3255–3262.

32 Kamino, T.; Saka, H. A newly developed high-resolution hot stage and its application to materials characterization. *Microsc. Microanal. Microstruct.* **1993**, *4*, 127–135.

33 Kamino, T.; Yaguchi, T.; Konno, M.; Hashimoto, T. In situ high temperature TEM observation of interaction between multi-walled carbon nanotube and in situ deposited gold nanoparticles. *J. Electron Microsc.* **2005**, *54*, 461–465.